Original Article

MOLECULAR METABOLISM

Pgc-1α controls epidermal stem cell fate and skin repair by sustaining NAD^+ homeostasis during aging

Wesley Wong [1], Elizabeth D. Crane [1], Hui Zhang [1], Jiahe Li [2], Tovah A. Day [1], Alex E. Green [3], Keir J. Menzies [3], Justin D. Crane [1,*]

ABSTRACT

Objective: The epidermal barrier is renewed by the activation, proliferation, and differentiation of keratinocyte stem cells after injury and aging impedes this repair process through undefined mechanisms. We previously identified a gene signature of metabolic dysfunction in aged murine epidermis, but the precise regulators of epidermal repair and age-related growth defects are not well established. Aged mouse models as well as mice with conditional epidermal loss of the metabolic regulator peroxisome proliferator-activated receptor gamma coactivator-1 alpha (Pgc-1α) were used to explore the cellular pathways which control skin repair after injury and stress.

Methods: Aged mice or those with epidermal Pgc-1α deletion (epiPgc-1α KO) and young or *Pgc1a*$^{fl/fl}$ controls were subjected to wound injury, UVB exposure or the inflammatory agent TPA. *In vivo* and *ex vivo* analyses of wound closure, skin structure, cell growth and stem cell differentiation were used to understand changes in epidermal re-growth and repair resulting from aging or Pgc-1α loss.

Results: Aging impairs epidermal re-growth during wound healing and results in lower expression of Pgc-1α. Mice with conditional deletion of epidermal Pgc-1α exhibit greater inflammation- and UVB-induced cell differentiation, reduced proliferation, and slower wound healing. epiPgc-1α KO mice also displayed reduced keratinocyte NAD^+ levels, shorter telomeres, and greater poly ADP-ribosylation, resulting in enhanced stress-stimulated p53 and p21 signaling. When NAD^+ was reduced by Pgc-1α loss or pharmacologic inhibition of NAD^+ synthesis, there was reduced stress-induced proliferation, increased differentiation, and protection against DNA damage via enhanced epidermal shedding. Similarly, aged mice exhibit disrupted epidermal NAD^+ homeostasis and enhanced p53 activation, resulting in p21 growth arrest after wounding. NAD^+ precursor treatment restores epidermal growth from old skin to that of young.

Conclusions: Our studies identify a novel role for epidermal Pgc-1α in controlling epidermal repair via its regulation of cellular NAD^+ and downstream effects on p53-driven growth arrest. We also establish that parallel mechanisms are evident in aged epidermis, showing that NAD^+ signaling is an important controller of physiologic skin repair and that dysfunction of this pathway contributes to age-related wound repair defects.

Keywords Aging; Epidermis; Wound healing; NAD^+

1. INTRODUCTION

The skin epidermis defends against environmental hazards such as solar radiation, lacerations, and infections via coordinated responses that trigger dynamic tissue remodeling [1,2]. Healthy skin repair depends on balanced rates of epidermal stem cell (ESC) division and differentiation and disruptions in this equilibrium are implicated in diseases such as psoriasis, eczema, skin cancer and slow-healing wounds [3]. Poor wound repair in the elderly represents an especially pressing health problem as the mechanisms underlying this pathology are not known and we lack effective healing therapies for the geriatric population [4]. Thus, identifying the triggering events which govern ESC growth and differentiation responses can lead to new ways to promote skin regeneration. Intriguingly, the epidermis deals with particularly high rates of intracellular DNA damage from UV exposure and genomic mutations are frequently found in otherwise asymptomatic skin [5], suggesting that ESCs have unique and effective mechanisms of shedding unfit or irrevocably damaged cells. However, the mechanisms by which this phenomenon is regulated in healthy skin is not understood.

A reduction in energy metabolites (i.e. ATP, glucose) activates sensitive stress—response pathways in tissues such as the liver or skeletal muscle to sustain organ function and bioenergetic disruptions are connected to a variety of disorders including diabetes [6], aging [7] and fatty liver disease [8]. We recently discovered that aged ESCs exhibit a transcriptional signature of metabolic dysfunction [9], suggesting that restoring energy homeostasis might be a way of treating wound repair defects in the elderly. Metabolites can act as direct energy sources as well as participate in chromatin remodeling (i.e. acetylation using acetyl Co-A) or DNA repair (i.e. ADP ribosylation using NAD^+) [10],

[1]Department of Biology, Northeastern University, 360 Huntington Avenue, Boston, MA 02115, USA [2]Department of Bioengineering, Northeastern University, 360 Huntington Avenue, Boston, MA 02115, USA [3]Department of Biochemistry, Microbiology and Immunology, University of Ottawa, Canada

*Corresponding author. E-mail: j.crane@northeastern.edu (J.D. Crane).

Received May 24, 2022 • Revision received July 30, 2022 • Accepted August 11, 2022 • Available online 17 August 2022

https://doi.org/10.1016/j.molmet.2022.101575

enabling the tight coupling of cellular energy and transcriptional programming. Metabolites are also known to regulate stem cell function and fate decisions [11,12]. The epidermis experiences dynamic UV- or wound-induced bioenergetic changes [13,14] and recent work has identified metabolites, such as lactate and serine, which can govern ESC behavior [15,16]. However, the critical metabolite networks and downstream signaling pathways that respond to stress, control ESC fate and are essential for *in vivo* epidermal repair responses have not been well characterized.

The Pgc-1 family is composed of the transcriptional coactivators Pgc-1α, Pgc-1β and PRC that respond to energy fluctuations and regulate metabolic programs in many tissues and organs [17]. Pgc-1α has specifically been shown to be critical for stress-induced metabolic signaling in skin fibroblasts [18] and melanocytes [19], however its specific role in skin aging or ESCs had not been established. We find that Pgc-1α expression is reduced in aged epidermis in conjunction with impaired wound re-epithelialization. To gain a better understanding of Pgc-1α's impact on ESC function, we conditionally deleted its expression in adult mice. We found that Pgc-1α sustains NAD^+ metabolism and suppresses epidermal stem cell differentiation after wounding, inflammation, and UVB-based skin damage. Notably, reducing NAD^+ levels potently suppress keratinocyte growth and increases differentiation after stress, but has no impact on these metrics under baseline, homeostatic conditions. Moreover, reduced NAD^+ levels after Pgc-1α removal coincides with telomere shortening and increased poly ADP-ribosylation, which results in a more robust activation of pro-differentiation p53 signaling after stress. Aged epidermis exhibits similar NAD^+ disturbances and p53 activation as Pgc-1α loss, establishing NAD^+ as a regulator of *in vivo* ESC-driven skin repair. Collectively, these findings identify several new potential therapeutic targets for wound healing disorders in the elderly.

2. MATERIALS AND METHODS

2.1. Animal handling and care

Ppargc1a$^{fl/fl}$ mice were obtained from Jackson Labs (Jackson Labs #009666) and mated with Keratin14$^{Cre\text{-}ERT/+}$ mice (Jackson Labs #005107) to generate Keratin14$^{Cre\text{-}ERT/+}$ *Ppargc1a*$^{fl/fl}$ animals (epiPgc-1α KO) and *Ppargc1a*$^{fl/fl}$ only littermates (WT). In all experiments mice expressing the Cre transgene were hemizygous. To induce Cre recombination, tamoxifen was dissolved in 70% ethanol and applied topically to shaved dorsal skin daily for a total of 7 days as 5 mg/day following a treatment schedule of two days, followed by a two-day break (typically for the weekend), and then continued for 5 more days. Mice were 8–16 weeks old at the time of tamoxifen administration and were not used for experiments until at least 21 days after the last day of tamoxifen application. Male and female C57BL/6J mice were acquired from Jackson Labs (#000664) and used for aging comparisons, acute UVB exposure and skin explant experiments. For aging experiments, young mice were 3–4 months of age and old mice were 24–25 months of age. All mice were housed in independently ventilated cages maintained under controlled environmental conditions (12 h/12 h) light/dark cycle, 23 °C) in an AAALAC approved animal facility. Mice received chow food and water *ad libitum* and were euthanized by cervical dislocation. All animal procedures were conducted under the approval of the Northeastern University IACUC.

2.2. Genotyping, mRNA expression and mtDNA copy number

Ear punches were collected from mice at weaning (21 days of age) for genotyping of Ppargc1a flox or Keratin14-CreER. All qPCR, including high resolution melt (HRM), was performed on a QuantStudio 3 instrument (ThermoFisher) as previously described [20]. Genomic DNA was extracted from ear tissue by adding 15 μL of QuickExtract DNA extraction solution (EpiCentre) and heating for 65 °C for 6 min followed by 98 °C for 2 min in a heat block. After centrifugation, 10 μL of sample was diluted 1:25 in ultrapure water for PCR analysis. Ppargc1a lox p sites were genotyped with HRM PCR using primer sequences provided by Jackson Labs. Primers — *Ppargc1a flox* forward: TCC AGTAGGCAGAGATTTATGAC; *Ppargc1a flox* reverse: TGTCTGGTT TGACAATCTGCTAGGTC. The presence or absence of the Keratin14-CreERT transgene was genotyped by SYBR qPCR using primer sequences provided by Jackson Labs — *Keratin14-CreER* forward: CGCATCCCTTTCCAATTTAC; *Keratin14-CreER* reverse: GGGTCCATGGT GATACAAGG.

For mRNA expression and DNA analysis, epidermis was separated from dermis using dispase (Roche) enzymatic digestion for approximately 60–90 min at 37 °C. After digestion, the epidermis was scraped and isolated using a scalpel blade and immediately frozen at −80 °C until later analysis. RNA was extracted from digested epidermis by homogenizing in TRIzol (Invitrogen) reagent with a bead mill apparatus (MPBio 5G). RNA was purified from TRIzol using a commercial column purification kit (Zymo Direct-zol RNA mini prep), with on-column DNase treatment and subsequent elution. Total RNA was then reversed transcribed to cDNA (ABI HC cDNA synthesis kit) and diluted in ultrapure water. The expression of mRNA was analyzed with qPCR using SYBR Green (*Nmnat1, Nmnat3, Kynu, Qprt, Nnmt, Ppargc1a*, *Sirt1*, *Parp1*, *Nampt*) or TaqMan chemistry (*Ppargc1b* (Mm00504720_m1), *Cox7b* (Mm00835076_g1), *Ndufs2* (Mm00467603_g1), and *Uqcr10* (Mm01187695_g1)). β2 microglobulin (*B2m,* Mm00437762_m1) was used as the housekeeping gene and its expression did not differ statistically between genotypes. Mouse liver samples were used a positive control for the epidermal qPCR analysis of *Kynu*, *Qprt* and *Nnmt*. SYBR primer sequences for mRNA expression are as follows:

Primer	Sequence
Nmnat1-forward	TGGCTCTTTTAACCCCATCAC
Nmnat1-reverse	TCTTCTTGTACGCATCACCGA
Ppargc1a-forward	AGCCGTGACCACTGACAACGAG
Ppargc1a-reverse	GCTGCATGGTTCTGAGTGCTAAG
Sirt1-forward	ATGACGCTGTGGCAGATTGTT
Sirt1-reverse	CCGCAAGGCGAGCATAGAT
Parp1-forward	TGGTTTCAAGTCCCTTGTCC
Parp1-reverse	TGCTGTCTATGGAGCTGTGG
Nampt-forward	AGCAGCAGAGCACAGTACCA
Nampt-reverse	GCTATCGCTGACCACAGACA
Nmnat3-forward	CAGTGGATGGAAACGGTGAAGG
Nmnat3-reverse	CAGAGGCTGATGGTGTCTTGCT
Qprt-forward	GAAAGACAACCATGTAGTGGCGG
Qprt-reverse	GGCTGCTACATTCCACCTCTAC
Kynu-forward	GTATGCGGATGGTAAAGCCACG
Kynu-reverse	CACTGAACAGGATCACGGCGAT
Nnmt-forward	CTTTGGGTCCAGACACTGTGCA
Nnmt-reverse	CCAGAGCCAATGTCAATCAGGAG

Dispase-digested epidermis was subjected to DNA extraction using a column purification kit (Zymo DNA isolation kit). After dilution to 1 ng/μL, the relative abundance of the mitochondrial DNA gene CoxII (MT–CO2) and single copy nuclear gene beta globin were assessed using the ratio of mtDNA:nDNA via qPCR. Similarly, relative telomere fragment length was assessed by qPCR and normalized to beta globin. Primer sequences are as follows:

Primer	Sequence
Telomere-Forward	CGGTTTGTTTGGGTTTGGGTTTGGGTTTGGGTTTGGGTT
Telomere-Reverse	GGCTTGCCTTACCCTTACCCTTACCCTTACCCTTACCCT
MT—CO2-forward	GCCGACTAAATCAAGCAACA
MT—CO2-reverse	CAATGGGCATAAAGCTATGG
Betaglobin-forward	GAAGCGATTCTAGGGAGCAG
Betaglobin-reverse	GGAGCAGCGATTCTGAGTAGA

2.3. In vivo skin stress and injury models

Full-thickness, splinted wound surgery was performed under isofluorane anesthesia as previously described [9]. Wounds were photographed daily using a DMC-FZ70 camera (Panasonic) and the Tegaderm dressing was changed daily until sacrifice. Wounded skin was affixed to a cardstock backing and fixed in 10% neutral buffered formalin for 24 h for later histological analysis. Additional mice were wounded in the same way and their wounds allowed to progress to full closure, as determined by daily macroscopic observation of the wound site.

TPA (12-*O*-tetradecanoylphorbol 13-acetate, LC labs, 81 μM) dissolved in acetone or acetone vehicle were each topically applied to the left or right half of shaved dorsal skin (100 μL per side) under isofluorane anesthesia. Skin samples were collected 48 h after TPA application. For all instances of acute UVB exposure, mice received ketamine/xylazine anesthesia (50 mg/kg ketamine; 5 mg/kg xylazine) i.p. and were exposed to a single dose of 200 mJ/cm^2 of UVB radiation using a dosimeter calibrated UV instrument (Tyler Research). The top and bottom dorsal skin were randomized for exposure to either UVB or were covered to serve as the sham control for each mouse. Tissue was collected at the indicated times after UVB exposure. In all experiments mice were given EdU (50 mg/kg) via intraperitoneal injection 3 h prior to sacrifice and tissue collection. For the UVB experiments, FK866 at 100 nM (Selleck Chemical, #S2799) or ethanol vehicle was applied topically applied immediate prior to and 24 h after a single dose of UVB radiation. Epidermal lysates for western blotting were collected by scraping 3 h after UVB treatment and a single dose of vehicle or FK866. Similarly, epidermal scrapes for NAD^+ measurement and fixed pieces of skin for histology were collected 48 h after UVB. Nicotinamide riboside (NR, ChromaDex, Los Angeles, CA, USA) at 500 mg/kg or PBS vehicle were intraperitoneally injected during wound healing and UVB experiments. With wound healing, NR or vehicle was injected once daily starting immediately after the completion of wound surgery until the skin was fully closed (re-epithelialized). With acute UVB, NR or vehicle was injected prior to and 24 h following UV and skin tissue collected 58 h after the initial UVB dose.

2.4. Keratinocyte explant culture

To prepare skin for keratinocyte culture, the dorsal skin of mice in the telogen phase was shaved using clippers and depilated with NAIR prior to skin collection. Skin was then excised, incubated for 2 min in a solution of povidone-iodine, twice in a solution of 70% ethanol (total of 2 min), and rinsed in sterile DPBS. Skin was then placed epidermis side down and scraped with a beveled scalpel blade to remove all subdermal adipose tissue and part of the dermal tissue. A 4 mm biopsy punch was used to excise individual tissue explants, which were then plated dermis side down into 24-well tissue culture plates (Thermo BioLite) followed by a 1 h drying period for explant adhesion to the surface. After the drying period, 400 μL of media (DMEM supplemented with 15% FBS, 1% glutamine, 1% penicillin, and 1% streptomycin) was added to submerge the explant. Explants from both genotypes were treated with and without nicotinamide (Acros Organics #NC1019639, 1 mM), nicotinamide riboside (Cayman Chemical, #23132, 1 mM), or nicotinamide mononucleotide (Cayman Chemical #16411, 1 mM), or for 72 h in a cell culture incubator at 37 °C with a 5% CO_2 atmosphere. Skin explants from wild-type C57BL/6J mice were treated with vehicle or increasing dosages of FK866 under the same culture conditions. All explants were prepared for imaging first by fixation with 10% neutral buffered formalin followed by staining with 0.1% crystal violet in a 30% methanol solution. The explants were then washed with water until the run-off was clear and imaged before drying out.

2.5. Sample lysis, western blotting and cytochrome c oxidase activity

Epidermal scrape samples were lysed in buffer containing 50 mM HEPES, 150 mM NaCl, 100 mM NaF, 10 mM Na pyrophosphate, 5 mM EDTA, 250 mM sucrose, 1 mM DTT, 1% Triton-X, and Pierce Protease and Phosphatase Inhibitor solution (Thermo Scientific). Samples were then freeze thawed 3 times using liquid nitrogen and passed through a 27-gauge needle to ensure complete lysis. The protein concentration of epidermal lysates was assessed using a BCA kit (Pierce). Equal amounts of protein were combined with loading buffer, boiled at 98 °C and then subjected to gel electrophoresis using 4—15% gradient gels (Bio-Rad). Separated proteins were then transferred to PVDF (Turboblot, Bio-Rad), blocked with 3% milk for 1 h, washed 3 times with TBS-T and incubated with primary antibody overnight at 4 °C. Primary antibodies were always diluted 1:1,000 in 5% fatty acid free BSA. After primary incubation, blots were again washed 3 times with TBS-T and incubated with HRP-linked secondary antibodies (Bio-Rad) at 1:5,000 dilution for 1 h at room temperature in 3% milk. Blots were developed using ECL (Clarity ECL substrate, Bio-Rad) and visualized using a computerized imaging system (ChemiDoc, Bio-Rad). Primary antibodies used were: Mono-/Poly-ADP ribosylation (MAR/PAR, mouse, Trevigen #4335-mc-100), pan-acetyl lysine (rabbit, Abclonal #A2391), Parp1 (rabbit, Cell Signaling #9542), VDAC (rabbit, Cell Signaling #4661), SDHA (rabbit, Cell Signaling #11998), TOM20 (rabbit, Santa Cruz #sc-11415), acetyl p53 (K382) (rabbit, Abclonal #A16324). β-actin antibody was used as a loading control and was obtained from Bio-Rad (VMA00048). Cox activity was also measured in epidermal lysates by monitoring the oxidation of sodium dithionite-reduced cytochrome *c* (Sigma Aldrich #C2506) via the change absorbance (550 nm at 30 °C) over 90 s using a plate reader. Activity was normalized to the protein content of the sample lysates used in the assay.

2.6. NAD^+ measurement

Pre-weighed tail epidermis, dorsal epidermal scrapes or liver tissue were lysed according to manufacturer recommendations for the NAD^+ detection kit (Promega NAD/NADH-Glo assay). Briefly, samples were homogenized in ice-cold base solution (0.2N NaOH (Fisher Scientific) +1% dodecyltrimethylammonium bromide (DTAB, Sigma Aldrich #D8638)) using a bead homogenizer (MPBio 5G). Using 100 μL of chilled extract, 50 μL of 0.4N HCl was added to all samples followed by heating at 60 °C for 15 min. Thereafter, 50 μL of 0.5 M Trizma base was added to each sample. Finally, samples were pipetted into white walled 96-well plates, combined with detection reagent, incubated for 30 min and the luminescence read using a plate reader (Synergy H1, Biotek). Relative NAD^+ levels were normalized to initial tissue weight.

2.7. Histology

Skin was fixed overnight in 10% neutral buffered formalin and thereafter transferred to 70% ethanol at 4 °C until processing. Samples were processed using an automated tissue processor (Thermo HistoStar, Kalamazoo, Michigan, USA) and embedded in paraffin wax. A microtome (Leica Biosystems, Buffalo Grove, Illinois, USA) was used to cut 4 μm skin cross-sections, which were allowed to dry overnight before de-waxing and further processing. Heat induced epitope retrieval was performed on de-waxed slides with either citrate or Tris—EDTA buffer prior to immunofluorescence staining. Skin cross-sections were blocked for 30 min at room temperature in PBS plus 5% normal goat serum PBS, which was also the primary antibody diluent, unless the target was a phospho-protein in which case TBS plus 5% normal goat serum was used. Primary antibodies and their usage were as follows: Keratin 14 (chicken, BioLegend #906004, 1:500, San Diego, California, USA), Keratin 10 (rabbit, BioLegend #905404, 1:500), Loricrin (rabbit, BioLegend #905104, 1:500), HMGB1 (rabbit, Abcam #ab79823, 1:250), p21 (rat, Abcam #ab107099, 1:100), thymine dimer (mouse, Novus #NB600-1141, 1:400), γH2AX (rabbit, Cell Signaling #9718, 1:40), Mono-/Poly-ADP ribosylation (MAR/PAR, rabbit, Cell signaling #83732, 1:500). Primary antibody incubations were carried out overnight at 4 °C. Following either PBS or Tris-buffered saline (TBS) wash, secondary detection antibodies conjugated with either AlexaFluor-647 or AlexaFluor-488 (Invitrogen, Carlsbad, California, USA) were diluted in either PBS or TBS at 1:250 were applied for 30 min at room temperature. EdU labeling was visualized using a Click-it chemistry kit (Invitrogen). ProLong Gold (Invitrogen) or ProLong Diamond (Invitrogen) with DAPI (4′,6-diamidino-2-phenylindole) were used interchangeably for mounting and allowed to cure prior to imaging. For thymine dimer staining, a mouse-on-mouse blocking kit (Vector Labs #BMK-2202, Burlingame, California, USA) was used per the manufacturer's instructions. Hematoxylin and Eosin staining was performed on 4 um de-waxed sections following standard histology protocols using Gill's Hematoxylin No.1 and Eosin Y (Sigma Aldrich). Colorimetric stained slides were mounted with Permount (Fisher Scientific, Pittsburgh, Philadelphia, USA). All brightfield imaging was done using an inverted EVOS XL (Life Technologies, Carlsbad, California) microscope. All fluorescence imaging was performed on a Revolve R4 (Echo Labs, San Diego, California, USA) microscope equipped with Olympus UPlanFL 10x/0.30, and UPlanFL 20x/0.50 air objectives using DAPI, FITC, Texas Red and Cy5 fluorescence channels.

2.8. Image analysis

All image processing and analysis was conducted using ImageJ FIJI (version 2.0.0-rc-69/1.52i, NIH), Photoshop CC 2019 (version 20.0.4, Adobe), and Illustrator CC 2019 (version 23.0.3, Adobe, San Jose, California, USA). For Hmgb1, MAR/PAR staining or p21 staining only, immunofluorescence images first underwent standardized thresholding of all samples to gate on only strongly positively stained cells followed by manual counting of positive cells for at least 3 unique fields from each sample. Nuclear Hmgb1-, p21-or MAR/PAR-positive cells were those that had overlapping signal with their nuclear DAPI signal. Nuclear size was measured the area of the DAPI signal in only basal layer epidermal cells in order to compare unstressed to stressed conditions (i.e. UVB, TPA) and were confirmed as Keratin 14 positive by co-staining. Keratin 14, Keratin 10, and Loricrin positive cells were those that had DAPI-associated cytoplasmic signal. Epidermal thickness measurements were performed on H&E stained intact skin cross-sections as previously described [21]. All histological analyses of intact skin only counted interfollicular epidermal cells and excluded hair follicles to maintain analytical consistency in fields with different amounts of follicles. Analyses of wounded skin used nascent hair follicles and the cut edge of the panniculus carnosus layer to identify the original wound margin. Keratin 14 tongue length was defined as the total length of the basement membrane of the Keratin 14 wound tongue spanning the leading edge to the first encountered hair follicle. Wound size measurements were obtained by planimetric analysis of overhead wound images in FIJI by measuring the non-re-epithelialized surface area relative to the initial surgery day. Images were calibrated using the 10 mm stainless steel ring or silicone ring used to splint open the wound as a coplanar scale reference. Briefly, a triangle was circumscribed around the wound diameter anchored to equidistantly spaced points around the splint. The area of the circumscribed triangle was used to transform the area of the wound to account for minor differences in imaging angle and distance within the camera images. Explant images were obtained by imaging the fixed and stained explants using a 4x objective under brightfield conditions on the Revolve R4 (Echo Labs, San Diego, California, USA) in the inverted configuration. For each explant, at least four image fields were captured to allow for panoramic stitching. Outgrowth areas were quantified on stitched images by using the pencil tool in ImageJ/FIJI and normalized to the similarly traced area of the original explant tissue.

2.9. Statistics

All data were analyzed in Prism 9 (GraphPad, San Diego, California, USA) using a student's *t* test or a two-way analysis of variance (ANOVA). Data were either log or square root transformed prior to statistical testing and any differences identified via ANOVA were assessed via a Tukey's post-hoc test to discern specific interaction effects. Statistical significance was set as $p < 0.05$.

2.10. Data availability statement

All data generated or analyzed in this study are included in the published article and its Supplementary Material Files.

3. RESULTS

3.1. Age-related impairments in wound healing and epidermal growth are associated with reduced Pgc-1α signaling

Aging produces well-characterized defects in wound healing whereby less epidermal re-growth is evident to the naked eye at day 8 and 9 after injury (macroscopic wound closure, Figure 1A). To assess specific defects in epidermal growth distinct from the other regenerating tissue layers (e.g. dermal fibroblasts), we employed a skin explant model of *in vitro* keratinocyte growth over 72 h in culture and find an approximately 60% reduction in outgrowth from aged skin (Figure 1B). Morphologically, the epidermal barrier is composed of stratified layers of keratinocytes that migrate upwards during terminal differentiation prior to being shed and Keratin 14-positive stem cells are primarily responsible for epidermal re-growth following skin injury (Figure 1C). To understand how early-stage epidermal re-growth was altered in the aged murine wound bed, we analyzed the active re-growth of the leading edge of the epidermis 5 days after injury, which precedes the time when we detect age-related healing differences macroscopically (i.e. day 8—9, see Figure 1A). In early day 5 wounds, we find that old mice have a shorter Keratin 14-positive epidermal tongue, as well as reduced proliferation (EdU labeling), which is indicative of slower re-growth (Figure 1D—F). To understand pathways which may control this repair, we sought to extend our published work showing a signature of metabolic dysfunction in aged ESCs, including a reduction in the nuclear regulator Pgc-1α [9]. We first confirmed these changes in aged epidermis via qPCR and found lower Pgc-1α mRNA in aged

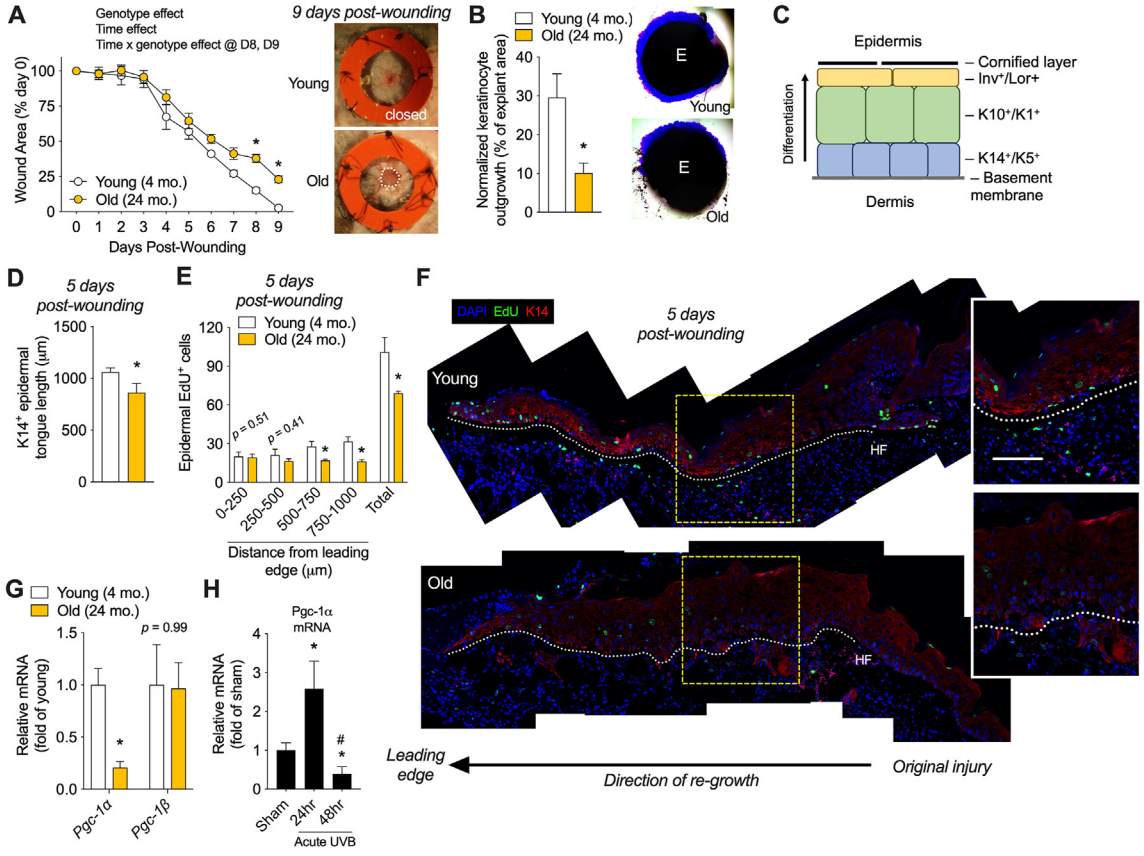

Figure 1: Aging results in slower wound healing and impaired epidermal stem cell growth in association with reductions in Pgc-1α signaling. (A) Wound closure over 9 days post-injury ($n = 6$—8, day 9 images at right) and (B) keratinocyte outgrowth ($n = 3$) from Young (4 mo. old) and Old (24 mo. old) C57/Bl6 mice. Cell growth in (B) was stained using crystal violet to ease visualization. (C) Illustration of the layer stratification of the epidermis and its markers. (D) Average Keratin-14 positive epidermal tongue length in young and old skin 5 days after wound injury with representative immunofluorescence images. $n = 5$—7. (E) EdU $^{+}$ cells in the right side of the epidermal leading edge of the healing wound bed of young and old mice 5 days after injury. $n = 4$—5. (F) Representative images of the wound epidermis from young and old mice with the white dotted line showing the first 1000 μm of the regenerated cells and bottom arrow indicates the tissue orientation. Yellow box marks inset region that has been magnified at right. (G) qPCR data of Pgc-1α and Pgc-1β mRNA in epidermis of young and old mice. (H) Epidermal Pgc-1α mRNA at 24 and 48 h following acute UVB exposure relative to sham control in young mice. Data are plotted as individual values or as mean ± SEM. Data were analyzed using a two-tailed students *t*-test (B, D, E, G), one-way ANOVA (H) or a two-way ANOVA followed by tukey's post-hoc test (A). *Significant difference ($p < 0.05$) from Young or Sham group. #Significant difference from 24 h UVB group. E, explant; HF, hair follicle. Scale bar in E is 100 μm.

versus young epidermis, however there were no changes in its homolog Pgc-1β (*Ppargc1b*; Figure 1G). We also assessed changes in Pgc-1α in young epidermis after acute UVB exposure, the most mutagenic wavelength of solar radiation, and found Pgc-1α mRNA (*Ppargc1a*) is upregulated 24 h after acute UVB exposure but becomes downregulated after 48 h (Figure 1H). Overall, epidermal Pgc-1α signaling is reduced during aging in conjunction with slower cellular re-growth and dynamically responds to UV stress. However, the functional role of Pgc-1α in the epidermis is not known.

3.2. Deletion of epidermal Pgc-1α reduces stress-induced proliferation, enhances differentiation and results in slower wound healing

To determine the role of epidermal Pgc-1α, we crossed tamoxifen-inducible *Keratin 14-CreER* mice with floxed Pgc-1α mice to generate *Keratin 14-CreER*; *Ppargc1a*$^{fl/fl}$ (epiPgc-1α KO) and *Ppargc1a*$^{fl/fl}$ littermates (WT). Upon tamoxifen exposure, cre expression induces recombination within epidermal Keratin 14^{+} basal cells, including all epidermal stem cells (ESCs) and any resulting differentiated progeny (Figure 2A). After tamoxifen we found a substantial reduction in epidermal mRNA expression of Pgc-1α (*Ppargc1a*) in WT relative to epiPgc-1α KO mice (Figure 2B). To determine whether Pgc-1α was necessary to sustain homeostatic epidermal structure, we assessed epidermal thickness as well as keratin 14 (K14, containing ESCs), keratin 10 (K10, spinous layer — differentiating keratinocytes) and loricrin (Lor, granular layer — differentiated keratinocytes) in intact, undamaged skin in both genotypes. We found no differences in total epidermal thickness (Supplemental Figure S1A), its stratification into differentiated layers (Figure 2C), or proliferation (EdU labeling) in WT and epiPgc-1α KO mice (Supplemental Figure S1B), demonstrating that Pgc-1α does not regulate epidermal proliferation or stratification of unstressed skin. Since Pgc-1α governs mitochondrial biogenesis in organs such as skeletal muscle [22], we next assessed whether its loss impacted epidermal mitochondrial abundance. However, we found no differences between WT and epiPgc-1α KO mice in epidermal mitochondrial gene expression (*Cox7b*, *Ndufs2*, and *Uqcr10*) or in the expression of Pgc-1β (*Ppargc1b*) (Supplemental Figure S1C). There were also no differences in protein expression (VDAC, SDHA, and TOM20, Supplemental Figure S1D) in unstressed epidermis. Similarly, we found equivalent epidermal cytochrome *c* oxidase activity and

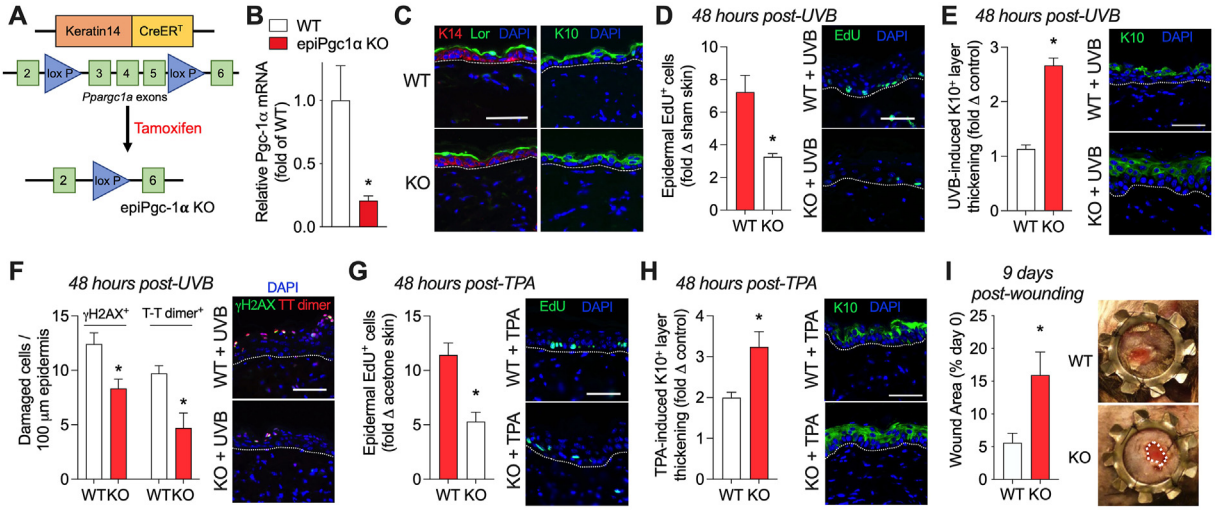

Figure 2: The genetic loss of epidermal Pgc-1α reduces cell growth and enhances differentiation after physiologic skin damage. (A) Schematic of cre-lox recombination to delete Pgc-1α in keratinocytes. (B) Epidermal Pgc-1α mRNA (*Ppargc1a*) in an *n* of 7–9 WT and epiPgc-1α KO mice. (C), representative images of keratin 14 (K14), keratin 10 (K10), and loricrin (Lor). (D) The UVB-induced fold-change in EdU$^+$ epidermal cells ($n = 5–6$) and (E) K10 layer thickness ($n = 4–7$) relative to sham skin in WT and epiPgc-1α KO mice. (F), quantification of γH2AX and thymine dimers in UVB exposed epidermis with representative images at right from an *n* of 5 WT and epiPgc-1α KO mice. (G) TPA-induced fold-change in EdU$^+$ epidermal cells ($n = 5–7$) and (H) K10 layer thickening ($n = 6–9$) relative to control skin in WT and epiPgc-1α KO mice. (I) The open wound area after 9 days in an *n* of 7–8 WT and epiPgc-1α KO mice. All data are plotted as mean ± SEM. All data were analyzed using an unpaired two-tailed students *t*-test. *Significantly different ($p < 0.05$) from WT. Scale = 50 μm for C–H.

mitochondrial DNA (mtDNA) copy number in WT and epiPgc-1α KO mice (Supplemental Figure S1E–F), demonstrating that Pgc-1α does not govern mitochondrial mass in the skin epidermis.

Given the dynamic changes in Pgc-1α mRNA after UVB exposure, we next determined the requirement of keratinocyte Pgc-1α in governing physiologic skin damage. We assessed acute UVB responses 48 h after stimulation and found no genotype differences in the extent of total epidermal thickening from sham skin (Supplemental Figure S2A). However, we found a reduced induction of proliferation (Figure 2D), increased thickening of the differentiated K10$^+$ layers (Figure 2E), and a higher number of nucleated loricrin$^+$ corneal cells (Supplemental Figure S2B) in UVB exposed epiPgc-1α KO epidermis versus WT, demonstrating disrupted keratinocyte growth responses. Since increased differentiation and cell shedding might accelerate the removal of damaged cells, we also stained for the DNA damage markers thymine dimers and γH2AX and we found fewer cells expressing these markers in UVB exposed epiPgc-1α KO compared to WT epidermis (Figure 2F). To determine whether the greater differentiation found in Pgc-1α null animals occurred in response to other stimuli, we topically applied the phorbol ester TPA which models acute inflammation similar to psoriasis [23]. TPA induces keratinocyte proliferation and differentiation but, in contrast to UVB exposure, does so without inducing apoptosis or DNA double strand breaks [24]. Similar to UVB, TPA treatment resulted in a lower induction of proliferation (Figure 2G), greater K10$^+$ layer thickening (Figure 2H) and produced more nucleated loricrin$^+$ cells in epiPgc-1α KO mice after 48 h (Supplemental Figure S2C). Since ESCs are a necessary component of the multicellular repair process after wound trauma [1,25], we also analyzed skin healing 9 days after surgical, full thickness wound injury. We found that wounds from epiPgc-1α KO mice remained more open at day 9 post-injury compared to WT mice, indicating slower re-epithelialization (Figure 2I). To corroborate this finding, we stained wound cross-sections from 9 days post-injury with H&E. We observed that WT wounds were fully re-epithelialized with a thicker nascent epidermis, but epiPgc-1α KO wounds exhibited a thin, partially re-grown epidermis (Supplemental Figure S2D). Finally, we sought to understand whether the slower epidermal repair of epi-Pgc1α KO mice was cell autonomous using a skin explant model of *in vitro* keratinocyte outgrowth and found that outgrowth was reduced by ~50% in epi-Pgc1α KO vs. WT skin (Supplemental Figure S2E). Collectively, this shows that Pgc-1α is broadly required to control stress-induced keratinocyte growth and sustain timely skin repair.

3.3. Pgc-1a sustains epidermal NAD$^+$ homeostasis and the pharmacologic inhibition of NAD$^+$ salvage promotes UVB-induced differentiation and protects against DNA damage

The coenzyme nicotinamide adenine dinucleotide (NAD$^+$) acts as an essential redox metabolite that participates in glycolysis and mitochondrial electron transport but can also be consumed by other processes such as DNA repair and histone deacetylation [26]. Pharmacologic inhibition of Nampt, the rate limiting enzyme of the NAD$^+$ salvage pathway that converts nicotinamide (NAM) to nicotinamide mononucleotide (NMN), has been shown to sensitize human keratinocytes to calcium-induced differentiation *in vitro* [27]. Pgc-1α has also previously been shown to sustain NAD$^+$ salvage via Nampt in the kidney [28], so we reasoned it may underlie the pro-differentiation phenotype in Pgc-1α null epidermis. We therefore measured the epidermal expression of genes related to salvage of NAD$^+$ from NAM (*Nmnat1, Nmnat3*, *Nampt*), NAM degradation (*Nnmt*) as well as NAD$^+$ consumption (*Parp1*, *Sirt1*). We found an increase in epidermal *Nampt*, a trend for greater *Nmnat1* ($p = 0.067$) and elevated *Parp1* expression in epi-Pgc1α KO animals, without any change in *Sirt1* or *Nmnat3* mRNA (Figure 3A). However, while *Nnmt* mRNA was highly expressed in murine liver, it was not detected in any epidermal samples. We also

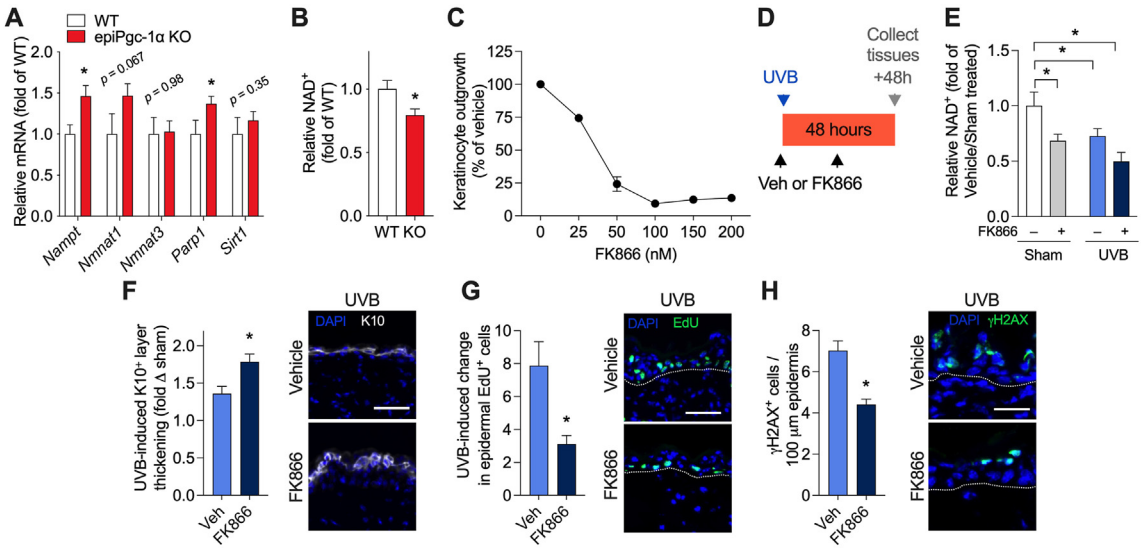

Figure 3: Pgc-1α null keratinocytes have disrupted NAD$^+$ metabolism and pharmacological inhibition of NAD$^+$ synthesis is sufficient to reduce proliferation and enhance UVB-induced differentiation. (A) Relative epidermal mRNA expression of genes related to NAD$^+$ metabolism from an *n* of 7–9 WT and epiPgc-1α KO mice. (B) Relative levels of NAD$^+$ in tail epidermis from an *n* of 4–5 WT and epiPgc-1α KO mice. (C) Dose response of *in vitro* keratinocyte outgrowth after 72 h from young skin explants in response to the Nampt inhibitor FK866 from an *n* of 2 biological replicates. (D) Schematic of the FK866 application combined with UVB stress in C57/Bl6 mice. (E) Epidermal NAD$^+$ levels, (F) Keratin 10 layer thickening, (G) the change in epidermal proliferation (EdU), and (H) the abundance of γH2AX positive epidermal cells of an *n* of 5–6 mice per group treated with topical FK866 (100 nM) or vehicle (Veh; ethanol) 48 h after sham or UVB exposure. Representative immunofluorescent images (F–H) are shown at right of quantification. All data are presented as mean ± SEM. Data were analyzed using a two-tailed Students *t*-test (A, B, F–H) or a two-way ANOVA followed by tukey's post-hoc test (E). *Significant difference ($p < 0.05$) from WT or Vehicle. Scale = 50 μm for F, G, H.

assessed the expression of enzymes involved in *de novo* NAD$^+$ synthesis (Quinolinate phosphoribosyl transferase- *Qprt*, kynureninase- *Kynu*), which is considered a liver-specific pathway [29], since this metabolism has not been examined in skin. We found no differences in *Kynu* expression in WT and epi-Pgc1α KO epidermis and *Qprt* was not detectable in any samples (Supplemental Figure S2F). We next assessed NAD$^+$ levels in tail epidermis, which is also derived from Keratin 14$^+$ precursors, to more accurately normalize to tissue weight. We found that NAD$^+$ was significantly reduced in epiPgc-1α KO vs WT tail epidermis (Figure 3B). Thus, Pgc-1α is necessary to sustain epidermal NAD$^+$ levels, however this does not appear to be due to a reduction in NAD$^+$ salvage.

To better understand the sensitivity of murine keratinocyte outgrowth to Nampt-dependent NAD$^+$ synthesis, we performed a dose response using the Nampt inhibitor FK866 *in vitro* using skin from C57BL/6J mice. We found that outgrowth was very sensitive to Nampt inhibition and doses of FK866 > 25 nM partially or fully inhibited growth (Figure 3C). To extend our findings from epiPgc-1α KO mice and to understand whether Nampt inhibition alone impacts UV-driven epidermal differentiation *in vivo*, we pre-treated WT mice with FK866 (100 nM) or vehicle topically: once immediately prior to UVB and a second dose 24 h following UVB exposure (Figure 3D). We collected skin 48 h after UVB and found that FK866 pre-treatment reduced epidermal NAD$^+$ levels irrespective of UVB or sham treatment (Figure 3E). In addition, skin without Nampt inhibition (vehicle) experienced UVB-induced reductions in NAD$^+$ (Figure 3E). Notably, FK866 treatment did not impact differentiation or proliferation in sham skin without UVB exposure, however it enhanced UVB-driven K10$^+$ layer thickening, lowered proliferation (EdU$^+$ cells), and reduced the number of γH2AX$^+$ cells in UVB exposed epidermis (Figure 3F–H). Thus, pharmacologically reducing NAD$^+$ synthesis via Nampt is sufficient to reduce proliferation and increase ESC differentiation after UVB stress *in vivo* as well as protect against DNA damage.

3.4. Increasing NAD$^+$ levels in Pgc-1a null mice rescues aberrant stress-induced differentiation and restores wound healing

Reduced cellular NAD$^+$ levels are linked to the aging of various tissues, and NAD$^+$ precursor supplementation can restore impaired tissue function and confer longevity in mice [30]. However, the impact of boosting NAD$^+$ on ESC-driven skin repair has not been established. To test if increasing NAD$^+$ levels could reverse the repair defects in epiPgc-1α KO mice, we treated skin explants from each genotype with vehicle control or 1 mM of the NAD$^+$ metabolite precursors nicotinamide (NAM), nicotinamide riboside (NR) or nicotinamide mononucleotide (NMN), established methods of increasing cellular NAD$^+$ [31]. We found that keratinocyte outgrowth *in vitro* was lower in vehicle treated epiPgc-1α KO explants compared to WT, however NMN, NAM and NR treatment increased outgrowth in epiPgc-1α KO explants only, restoring it to that of WT (Figure 4A and C). Moreover, when the effect of NAD$^+$ precursors was normalized to the paired vehicle treatment of each mouse, growth changes were greater from epiPgc-1α KO compared to WT explants (Figure 4B–C). We then tested whether treating epiPgc-1α KO mice daily with NR (500 mg/kg i.p.) starting at the time of wounding could restore epidermal NAD$^+$ levels and rescue skin healing defects *in vivo*. As expected, NR treatment increased NAD$^+$ in the liver of both genotypes to a similar extent versus vehicle control mice (Figure 4D), demonstrating comparable systemic delivery of NR. Additionally, we again found lower NAD$^+$ in the tail epidermis of vehicle-treated epiPgc-1α KO vs. WT mice ($p = 0.057$), however NR treatment significantly increased NAD$^+$ levels in epiPgc-1α KO tail epidermis such that the levels were comparable to NR-treated WT mice (Figure 4E). Importantly, we found that NR treatment reduced the

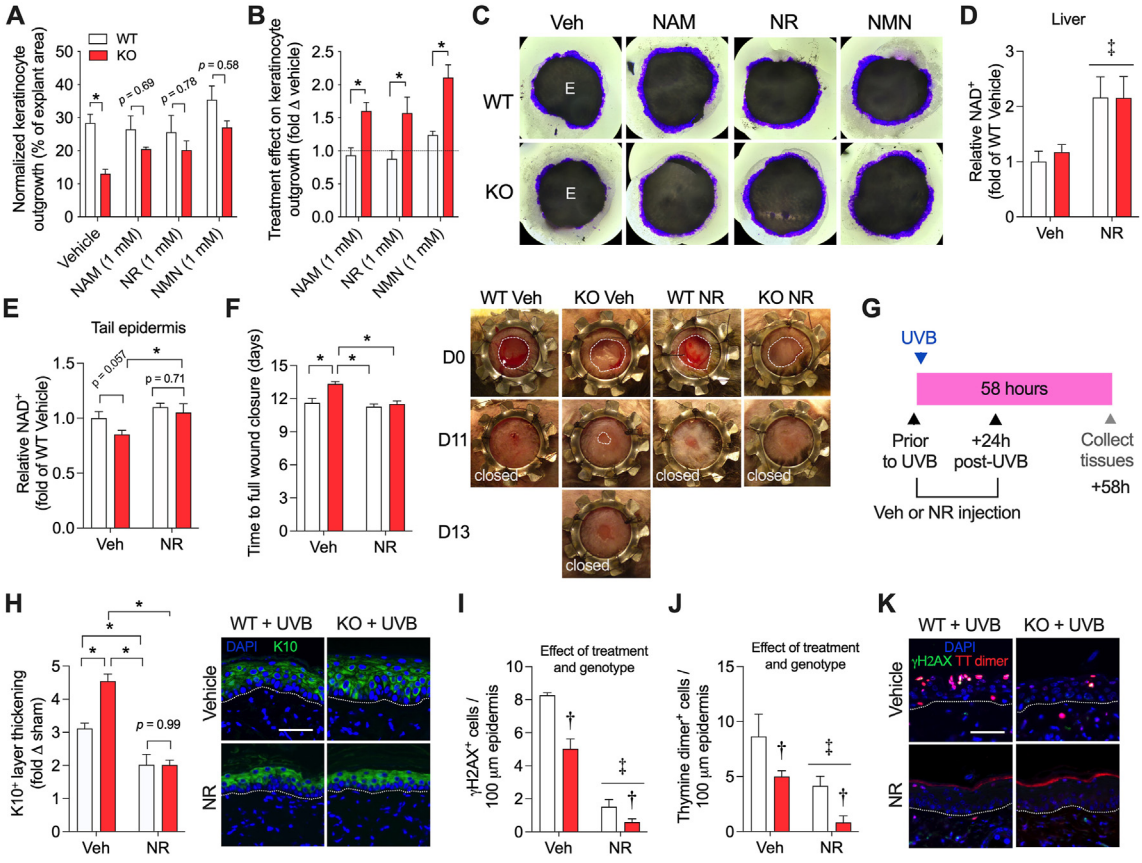

Figure 4: Treating epidermal Pgc-1α KO mice with NAD$^+$ precursors speeds skin healing and suppresses UVB-induced differentiation. (A—B) Keratinocyte outgrowth as a fraction of explant area or as fold of vehicle condition using an *n* of 4 WT and epiPgc-1α KO skin samples treated with or without the NAD$^+$ precursors nicotinamide mononucleotide (NMN), nicotinamide (NAM) or nicotinamide riboside (NR). (C) Representative images of outgrowth from (A—B) stained using crystal violet to ease visualization. (D—F), Liver NAD$^+$, tail epidermis NAD$^+$ levels and time to full wound closure in an *n* of 4—7 WT and epiPgc-1α KO mice injected daily with vehicle or 500 mg/kg NR. Representative images from day 0 (D0), day 11 (D11) and day 13 (D13) post-injury. (G) Schematic of UVB exposure and NR dosing. (H—K) Keratin 10 thickening, γH2AX$^+$ cells and thymine dimer$^+$ cells in UVB-exposed epidermis from an *n* of 4 WT and Pgc-1α KO mice treated with vehicle or nicotinamide riboside (NR). Representative immunofluorescent images (H, K) are shown at right of quantification. All data are plotted as mean ± SEM. Data were analyzed using a two-tailed Student's *t*-test (A—B) or a two-way ANOVA followed by tukey's post-hoc test (D-F, H-J). *Significant difference ($p < 0.05$) from WT or the indicated group. Significant effect ($p < 0.05$) of group (‡) or treatment (†). E, explant. Scale bar = 50 μm in (H), (K).

time required for full wound closure (complete re-epithelialization) by ~2—3 days in epiPgc-1α KO mice, without any impact on the healing rate of WT healing mice (Figure 4F). We also analyzed the effect of NR treatment on UVB-induced differentiation in a separate cohort of WT and epiPgc-1α KO mice treated with NR (500 mg/kg i.p.) or vehicle immediately prior to UVB as well as 24 h later (Figure 4G). Notably, NR treatment had no impact on K10$^+$ layer thickness in sham treated skin in either genotype (data not shown). Vehicle-treated epiPgc-1α KO mice again had greater UVB-driven K10$^+$ layer thickening than WT mice, however, NR administration reduced this differentiation in both WT and epiPgc-1α KO mice such that the genotype differences were ablated (Figure 4H). We also assessed DNA damage and found that there were fewer overall UVB-induced γH2AX$^+$ and thymine dimer$^+$ cells in epiPgc-1α KO mice and there was an overall lowering effect of NR treatment on DNA damage (Figure 4I—K), likely because NAD$^+$ is a substrate for DNA repair enzymes such as Poly-ADP ribosylases (Parps) [32]. This demonstrates that restoring keratinocyte NAD$^+$ can rescue wound healing and inhibit excessive UVB-induced epidermal differentiation in Pgc-1α null skin.

3.5. Loss of Pgc-1α induces telomere shortening, augments Parp activity and enhances stress-induced p53 signaling

We next sought to understand the pathways responsible for reduced NAD$^+$ levels in epiPgc-1α KO mice. We measured mono- and poly-ADP ribosylation (MAR/PARylation) abundance in epidermal lysates via western blotting to approximate changes in PARPs and found greater MAR/PARylation in epiPgc-1α KO vs. WT epidermis (Figure 5A). However, we did not observe changes in total Parp1 protein expression (Supplemental Figure S3A), which is the predominant enzyme of NAD$^+$-dependent PARylation [33]. To understand whether MAR/PARylation was elevated in all cells or was due to an increase in the number of cells with high Parp activity, we assessed MAR/PARylation in skin cross-sections using IHC. We found that epiPgc-1α KO mice had a greater abundance of bright MAR/PAR$^+$ epidermal nuclei versus WT (Figure 5B). Since sirtuin-mediated lysine de-acetylation of histones is also a major consumer of cellular NAD$^+$ [31], we measured acetyl lysine abundance and found it was increased in epiPgc-1α KO vs. WT epidermal lysates (Figure 5C), showing that the low NAD$^+$ levels after Pgc-1α loss coincided with greater lysine acetylation.

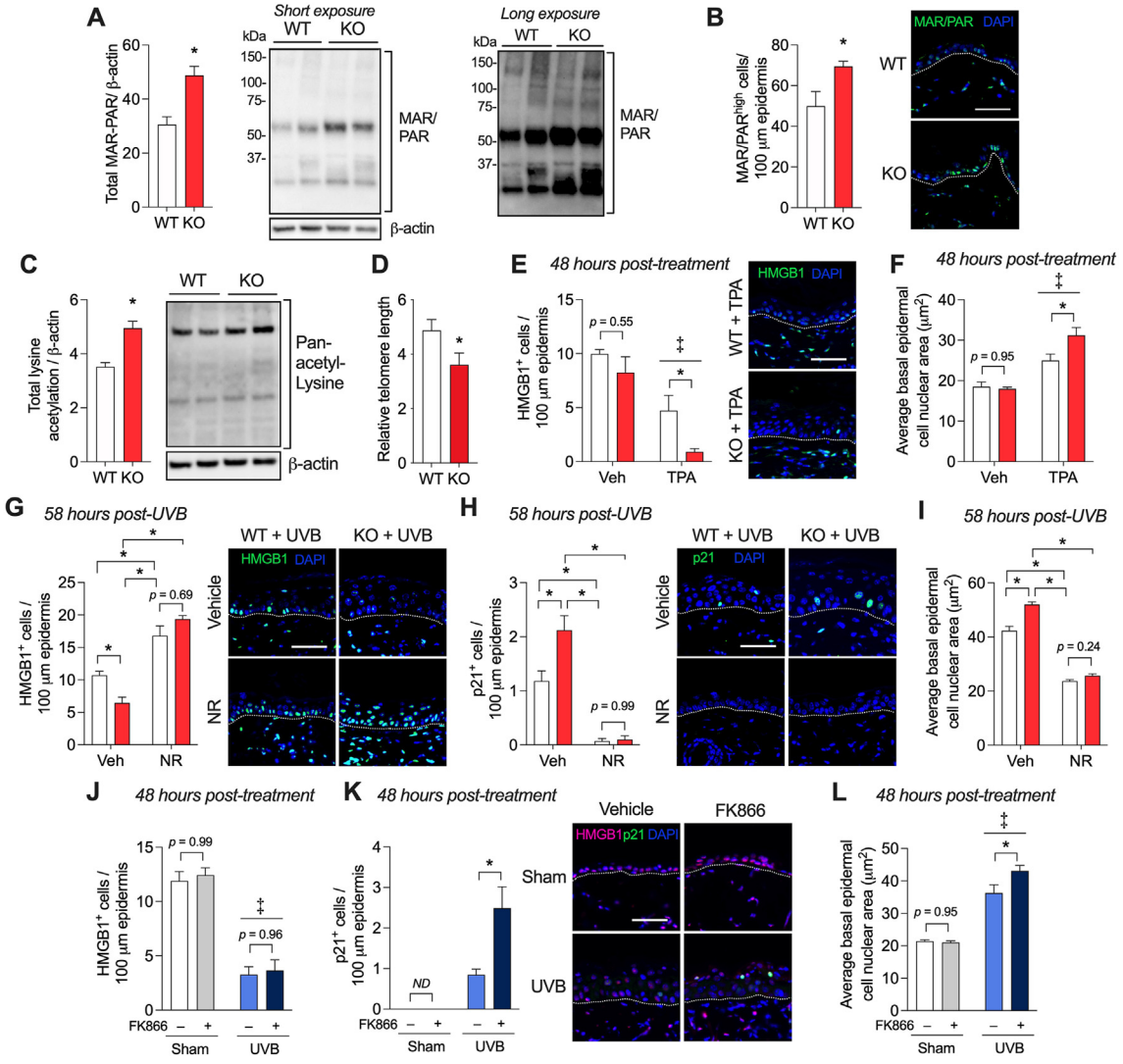

Figure 5: Telomere dysfunction after epidermal Pgc-1α loss sensitizes stem cells towards stress-induced p53 activation and nuclear enlargement in an NAD$^+$-dependent manner. (A) Quantification of immunoblotting of poly- and mono-ADP ribose (MAR/PAR) in epidermal lysates from an *n* of 6—7 WT and epiPgc-1α KO mice. (B) The number of brightly stained MAR/PAR epidermal cells (MAR/PAR^{high}) from an *n* of 4—6 WT and epiPgc-1α KO mice. (C) Quantification of immunoblotting of pan-acetyl lysine in epidermal lysates from an *n* of 6—7 per group. (D) Mean epidermal telomere length from an *n* of 8 per group. (E) Nuclear HMGB1$^+$ cells and (F) basal layer nuclear size in vehicle and TPA treated skin in an *n* of 5—6 WT and epiPgc-1α KO mice. (G) Nuclear HMGB1$^+$ or (H) p21$^+$ epidermal cells ($n = 4$—5) as well as (I) basal layer nuclear size ($n = 3$) in UVB-exposed epidermis after 58 h from WT and epiPgc-1α KO mice treated with vehicle or nicotinamide riboside (NR, 500 mg/kg). (J) Nuclear HMGB1$^+$ or (K) p21$^+$ epidermal cells as well as (L) basal layer nuclear size in sham and UVB-exposed epidermis in an *n* of 6 C57Bl/6 mice treated with topical vehicle or FK866. Representative immunoblotting (A, C) or immunofluorescent images (B, E, G, H, K) are shown at right of quantification. All data are plotted as mean ± SEM. Data were analyzed using a two-tailed Student's *t*-test (A—D) or a two-way ANOVA followed by tukey's post-hoc test (E—L). *Significant difference ($p < 0.05$) from WT or the indicated treatment group. ‡Significant ($p < 0.05$) effect of treatment. ND, not detectable. Scale bars = 50 µm in B, E, G, H, K.

Similarly, we found that inhibiting NAD$^+$ synthesis using topical FK866 drove increased epidermal lysine acetylation 3 h following UVB exposure (Supplemental Figure S3B). To understand what might be driving increased baseline MAR/PARylation, we measured telomere length via qPCR and found it was decreased in the unstressed epidermis of epiPgc-1α KO vs. WT mice (Figure 5D). Since telomere shortening can induce p53/p21 signaling [34] and activation of this axis enhances the terminal differentiation of keratinocytes during proliferative stress [35], we quantified both nuclear p21-and HMGB1-positive cells, the latter of which is lost from the nucleus after p53 activation [36]. Additionally, during our experiments we noticed that there were frequently very large basal layer nuclei present in the stressed epidermis of epiPgc-1α KO mice (see Figures 2E,H and 4H). Nuclear size has been shown to mark liver cells with telomere dysfunction and p21 upregulation [37], so we also measured epidermal nuclear size adjacent to the basement membrane. Although Pgc-1α loss produced baseline telomere shortening and higher MAR/PARylation, we found no changes in HMGB1 and an absence of p21 in unstressed skin (Figure 5E). However, inflammatory TPA stress enhanced p53 signaling via fewer nuclear HMGB1-positive cells and caused nuclear enlargement to a greater extent in epiPgc-1α KO vs. WT epidermis despite an absence of p21-positive cells after 48 h (Figure 5E—F). UVB treatment also reduced nuclear HMGB1 cells and enhanced nuclear size but resulted in increased p21-positive cells

after 58 h versus sham treatment; these effects were more pronounced in epiPgc-1α KO vs. WT epidermis (Figure 5G—I; similar effect on p21 at 48 h post-UVB (Supplemental Figure S3C)). Importantly, this more sensitive activation of p53/p21 signaling was NAD^+-dependent as NR treatment reduced p21-positive epidermal cells, lowered nuclear size and increased HMGB1-positive cells in UVB exposed skin from both genotypes such that NR-treated epiPgc-1α KO were equivalent to WT (Figure 5G—I). Interestingly, in sham skin without UVB exposure, NR treatment increased nuclear HMGB1-positive cells in both genotypes, suggesting a suppression of p53 activity, yet had no impact on nuclear size (Supplemental Figure S3D—E). Finally, we examined whether NAD^+ lowering alone was sufficient to cause greater sensitivity to stress-induced p53/p21 signaling in WT mice. We found that inhibition of NAD^+ salvage using topical FK866 did not impact UVB-induced nuclear HMGB1 loss, potentially due to the transient effects of chemical treatments, but it did augment p21 expression and nuclear enlargement compared to vehicle treatment after 48 h (Figure 5J-L). Thus, epidermal Pgc-1α loss or NAD^+ lowering promote a more sensitive induction of p53 signaling after multiple types of skin damage, although downstream p21 appears to be transduced in a stress-specific manner. Overall, this demonstrates an important role of epidermal Pgc-1α to protect NAD^+ homeostasis, which is essential for stem cell-driven skin repair as it behaves as a broad acting physiologic inhibitor of stress-induced p53 signaling.

3.6. Aged epidermis exhibits disturbed NAD^+ homeostasis and increased p21 growth arrest

With our new-found understanding of epidermal NAD^+ biology during skin repair, we sought to understand whether NAD^+ homeostasis and p53 signaling were similarly disrupted in aged mice. We found reduced NAD^+ levels in uninjured old versus young dorsal epidermis (Figure 6A). We also found altered mRNA expression of the NAD^+ consumers *Parp1* (increased 2-fold) and *Sirt1* (reduced ~50%), as well as an NAD^+ salvage enzyme (reduced *Nmnat1* ~60%), but no change in *Nampt or Nmnat3* (Figure 6B). There was also no difference in expression of the *de novo* NAD^+ synthesis enzyme *Kynu* in young and old epidermis ($p = 0.94$). Similar to our findings with epidermal Pgc-1α loss, we also found increased MAR/PAR levels and increased lysine acetylation in aged epidermal protein lysates (Figure 6C—D). This indicates that aging may enhance epidermal Parp activity and reduce Sirt activity. To understand how growth arrest may be augmented by reduced NAD^+ levels, we assessed the acetylation of p53 at K382, which is a specific target of Sirt1 whose expression sustains p53 driven cell cycle arrest [38]. Acetyl p53 (K382) was not

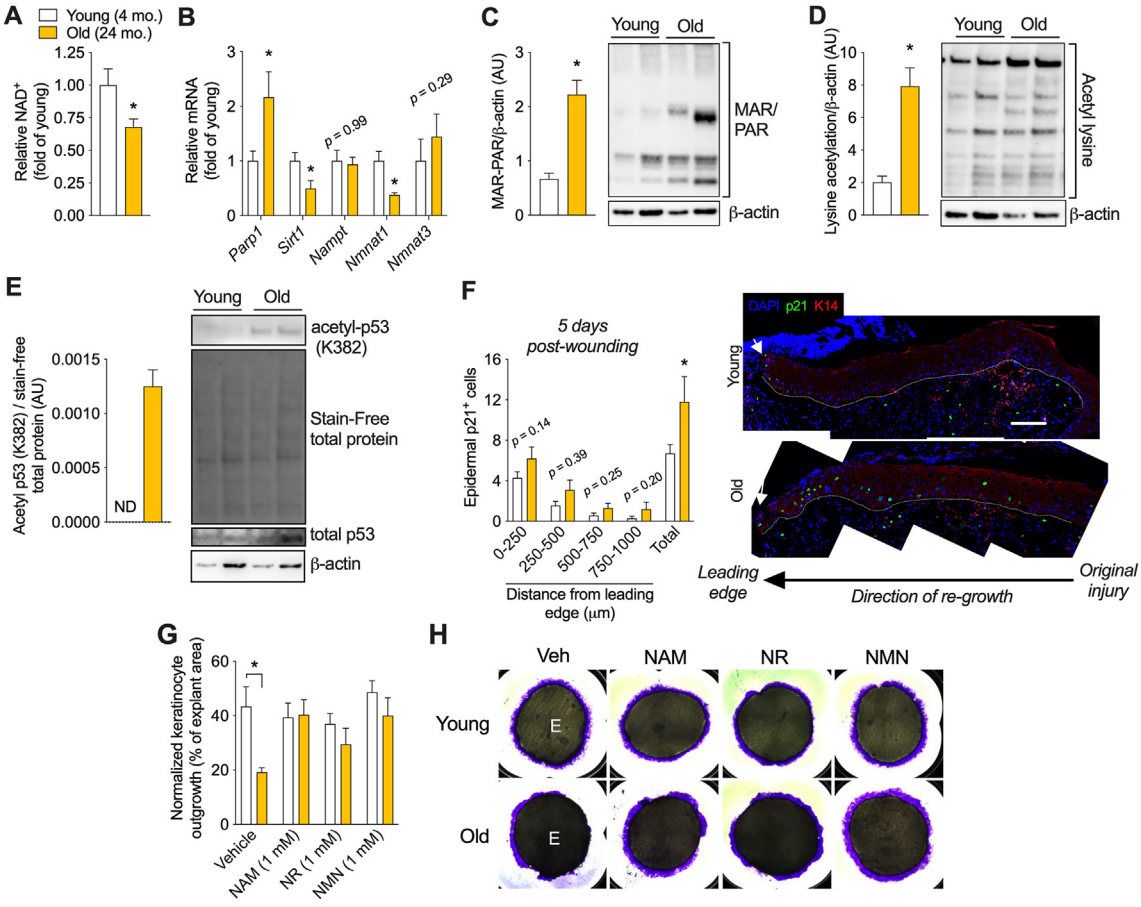

Figure 6: Aging disrupts epidermal NAD^+ homeostasis and augments the p53-p21 signaling axis. (A) Relative epidermal NAD^+ levels and (B) mRNA expression of NAD^+ metabolism-related genes in young vs. old mice. $n = 5$—7. Immunoblots of (C) MAR/PARylation, (D) lysine acetylation, and (E) acetyl p53 (K382) in young and old epidermis with quantification at right. $n = 3$—4. (F) Epidermal $p21^+$ cells within the leading edge 5 days after injury in young (4 mo.) and old (24 mo.) mice. $n = 5$—7. Representative images at right with dotted line showing the first 1000 μm of the leading edge which starts at the arrow. (G) Skin keratinocyte explant outgrowth from young and old mice treated with the indicated NAD^+ precursors for 72 h. (H) Representative images of keratinocyte outgrowth stained with crystal violet to ease quantitation. Data are shown as mean ± SEM. Data were analyzed using a two-tailed students *t*-test. Scale bar is 100 μm μm. *Significant difference ($p < 0.05$) from Young group.

detectable in young epidermal samples, however, all of the old samples had visible acetylated p53 bands (Figure 6E). To understand how p53 signaling might be altered by aging in healing wounds, we stained for the downstream p53 target p21, which is known to govern fibroblast proliferation in healing wounds as well as liver regeneration [39,40]. At 5 days post-wounding, we find a greater overall number of p21 positive cells in the first 1,000 um of the newly formed epidermal leading edge in aged mice (Figure 6F), suggesting that augmented p21 arrest may underlie epidermal growth and repair defects during aging. To examine whether restoring NAD^+ with precursors could reverse age-associated epidermal growth defects, we treated young and old skin explants with NAM, NR and NMN *in vitro*. Similar to our findings in epiPgc-1α KO skin, we found that keratinocyte outgrowth was reduced in vehicle treated explants from old versus young mice, but age-related growth defects were absent in NAM, NR or NMN treated conditions (Figure 6G–H). Thus, akin Pgc-1α loss or Nampt inhibition, aging disrupts epidermal NAD^+ homeostasis, augments p53/p21 activation and slows re-growth, but this is reversible after treatment with NAD^+ precursors.

4. DISCUSSION

The skin epidermis is an important environmental barrier, but the signaling networks that coordinate its energy levels, growth responses and stem cell fate decisions are not understood. Similarly, the mechanisms whereby aging impedes epidermal growth are also not clear, which limits our ability to therapeutically treat slow wound healing and other skin disorders in the elderly. In particular, wound healing requires the complex coordination of connective tissue, immune cells and epithelial cells for complete repair and we focused specifically on the epithelial mechanisms relevant to wound injury and other type of skin repair. Our findings center around epidermal NAD^+ metabolism, which is not well studied as prior research has largely focused on the control of DNA repair within keratinocytes *in vitro* [41,42] or in relation to tumor growth [43,44]. Based on our previous finding of metabolic dysfunction in aged ESCs [9], we found that the metabolic regulator Pgc-1α is reduced in aged epidermis and is dynamically altered after UVB exposure. After genetically deleting epidermal Pgc-1α, we identified the *in vivo* relevance of NAD^+ signaling in controlling cell growth after several types of physiologic stress in young, healthy skin. Moreover, we show that NAD^+ levels are sustained by Pgc-1α and control stress-induced p53/p21 signaling during skin repair and that this signaling axis is disrupted in the aged murine epidermis. Prior studies have linked telomere dysfunction to Pgc-1α and mitochondrial impairments using more severe degeneration in progeroid *Tert*$^{-/-}$ mice [45] or ApoE-null mice [46], however we show that Pgc-1α loss alone in adult epidermal stem cells can disrupt telomeres and NAD^+ levels without a strong impact on mitochondrial activity. We also establish that low NAD^+ levels are sufficient to reduce the overall proportion of DNA damaged cells and augment stress-induced p53 signaling due to differentiation-driven cell ejection from the skin. Thus, in the face of extensive genomic stress or p53 mutations, reduced NAD^+ can augment residual p53 activity and could help explain how human keratinocytes tolerate high rates of DNA mutagenesis without tumorigenesis [5] via the rapid ejection of damaged clones with low NAD^+. Our findings surrounding growth arrest agree with studies in other tissues where Pgc-1α has been implicated in suppressing vascular [46] and fibroblast [47] senescence. Interestingly, our findings more directly resemble the phenotypes resulting from the epidermal deletion of the mitochondrial antioxidant Sod2, which also enhances stress-induced keratinocyte differentiation and slows wound healing [48]. It is possible that the oxidative damage and metabolic disruptions induced by Sod2 loss impacted telomere length or NAD^+ homeostasis as this study also found increased cell cycle stalling after stress [48], but this requires further investigation.

While the importance of keratinocyte NAD^+ signaling to cell cycle stalling after UV damage *in vitro* is known [42,49], we extend these findings by showing that NAD^+-dependent signaling to p53 is also important for responses to epidermal wound injury or inflammatory stress (i.e. TPA) *in vivo*. In agreement, whole body Parp1 KO mice exhibit a hyper-proliferative epidermal phenotype with psoriatic IMQ treatment [50] and heal wounds more quickly [51], potentially due to increased NAD^+ availability when Parp1-driven consumption is lost. While these studies suggest that Parp1 is a major consumer of epidermal NAD^+ during proliferation and re-growth, however, given the complex orchestration of different cell types during skin repair, this should be confirmed using a more specific model of epidermal Parp1 loss. Our work also finds elevated MAR/PARylation from PARPs in concert with reduced NAD^+ in aged epidermis. This suggests that boosting NAD^+ levels could be used to speed wound healing in elderly individuals and that inhibiting PARP activity could help to achieve this response. However, NAD^+ biology is complicated and can be influenced by external factors such as increased cellular senescence [52,53], chronic inflammation [53,54] or changes in the microbiome [55] in conjunction with epidermal genomic damage [42]. As a result of inflammation or senescence, NAD^+ levels can be reduced via the NADase CD38, however CD38 is primarily expressed in immune cells such as macrophages [54], which are not found in the epidermis. Similarly, the amount of the NAD^+ precursor nicotinamide can be reduced via NNMT-driven methylation [56], however, we were unable to detect *Nnmt* expression in murine keratinocytes. Future work should identify the major consumers of epidermal NAD^+ or its precursors after skin damage and during aging as this could reveal additional avenues of therapy.

The precise cell cycle mechanisms by which aging slows wound healing are only beginning to be understood. An increased expression of the growth regulator $p16^{ink4a}$ has been implicated in inhibiting wound closure in young mice, largely within the dermis [57], however, we and other groups show little change in $p16^{ink4a}$ in aged murine epidermis [9,58]. Moreover, chronic $p16^{ink4a}$ overexpression unexpectedly promotes epidermal hyperplasia [59]. Alternatively, p21 has been shown to be transiently upregulated in aged fibroblasts during healing and may limit wound closure [39], but aging-induced changes in p21 within the healing epidermis had not been identified. In our studies, we extend these data by showing that epidermal p53/p21 signaling can be controlled by NAD^+ levels after stress. Moreover, the activation of epidermal p53/p21 signaling appears sensitized in old skin in conjunction with disrupted NAD^+ homeostasis yet is reversible. We reason that cell cycle stalling is only transient in aged wounds as they eventually fully re-epithelialize. However, more prolonged p21-driven stalling or permanent growth arrest via $p16^{inka}$ may be prevalent in the epidermis of non-healing diabetic skin ulcers which are highly inflamed and do not heal.

It is notable that we only observe physiologic responses to altered NAD^+ levels when it is combined with cellular stress. This suggests that low NAD^+ "primes" ESCs for growth arrest or differentiation but only triggers this process after additional physiologic stimuli such as DNA breaks, growth factors or increased calcium [1]. This may explain why the aged epidermis does not have a substantial structural phenotype during homeostasis, but the effects of aging become more evident after injury. This altered stress-response is most likely derived

from restricted NAD^+-dependent histone deacetylation (e.g. greater lysine acetylation) that promotes more "open" euchromatin, fitting with our observation that stress-induced nuclear enlargement and acetylation are controlled by NAD^+ levels. Interestingly, in the WT epidermis inflammatory stress from TPA treatment results in significantly less nuclear enlargement compared to UVB stress after 48 h (1.35 vs. ~1.7-fold increase), potentially due to a greater demand on NAD^+ and a more intensive repair process after UVB-driven DNA damage. While chromatin modifications of renewing and differentiating ESCs are well described [60], the NAD^+-dependent aspects of these networks have not been explored. Moreover, MAR/PAR moieties act as dynamic intracellular signals themselves, so future work should investigate their specific roles in stem cell-mediated tissue repair.

4.1. Conclusion

Overall, these results establish NAD^+ homeostasis as a critical facet of skin repair and as a sensitive rheostat of keratinocyte fate after physiologic stress. During aging, a disruption of NAD^+ levels may contribute to the increase in epidermal differentiation and slower wound repair evident in the elderly.

AUTHOR CONTRIBUTIONS

Conceptualization: WW, JDC, KJM, TAD; Data Curation: WW, JDC, EDC; Formal Analysis: WW, EDC, HZ, JDC; Funding Acquisition: JDC, JL; Investigation: WW, EDC, HZ, JDC; Methodology: WW, EDC, JDC; Project Administration: WW, EDC, JDC; Resources: JDC, TAD, JL; Supervision: JDC; Validation, WW, EDC, JDC; Visualization: WW, EDC, HZ; Writing — original draft: WW, JDC; Writing — review and editing: EDC, HZ, AEG, KJM, TAD, JL.

ACKNOWLEDGMENTS

This study was funded by startup funds from Northeastern University (Boston, MA) to Justin D. Crane and by NIBIB R21 EB030769-01A1 to Jiahe Li and Justin D. Crane.

CONFLICT OF INTEREST

The authors state no conflict of interest.

APPENDIX A. SUPPLEMENTARY DATA

Supplementary data to this article can be found online at https://doi.org/10.1016/j.molmet.2022.101575.

REFERENCES

[1] Rognoni, E., Watt, F.M., 2018. Skin cell heterogeneity in development, wound healing, and cancer. Trends in Cell Biology 28(9):709—722. https://doi.org/10.1016/j.tcb.2018.05.002.

[2] Dekoninck, S., Blanpain, C., 2019. Stem cell dynamics, migration and plasticity during wound healing. Nature Cell Biology 21(1):18—24. https://doi.org/10.1038/s41556-018-0237-6.

[3] Lopez-Pajares, V., Yan, K., Zarnegar, B.J., Jameson, K.L., Khavari, P.A., 2013. Genetic pathways in disorders of epidermal differentiation. Trends in Genetics 29(1):31—40. https://doi.org/10.1016/j.tig.2012.10.005.

[4] Gould, L., Abadir, P., Brem, H., Carter, M., Conner-Kerr, T., Davidson, J., et al., 2015. Chronic wound repair and healing in older adults: current status and future research. Wound Repair and Regeneration 23(1):1—13. https://doi.org/10.1111/wrr.12245.

[5] Jonason, A.S., Kunala, S., Price, G.J., Restifo, R.J., Spinelli, H.M., Persing, J.A., et al., 1996. Frequent clones of p53-mutated keratinocytes in normal human skin. Proceedings of the National Academy of Sciences 93(24):14025—14029. https://doi.org/10.1073/pnas.93.24.14025.

[6] Stump, C.S., Short, K.R., Bigelow, M.L., Schimke, J.M., Nair, K.S., 2003. Effect of insulin on human skeletal muscle mitochondrial ATP production, protein synthesis, and mRNA transcripts. Proceedings of the National Academy of Sciences 100(13):7996—8001. https://doi.org/10.1073/pnas.1332551100.

[7] Petersen, K.F., Befroy, D., Dufour, S., Dziura, J., Ariyan, C., Rothman, D.L., et al., 2003. Mitochondrial dysfunction in the elderly: possible role in insulin resistance. Science 300(5622):1140—1142. https://doi.org/10.1126/science.1082889.

[8] Sunny, N.E., Parks, E.J., Browning, J.D., Burgess, S.C., 2011. Excessive hepatic mitochondrial TCA cycle and gluconeogenesis in humans with nonalcoholic fatty liver disease. Cell Metabolism 14(6):804—810. https://doi.org/10.1016/j.cmet.2011.11.004.

[9] Wong, W., Crane, E.D., Kuo, Y., Kim, A., Crane, J.D., 2019. The exercise cytokine interleukin-15 rescues slow wound healing in aged mice. Journal of Biological Chemistry 294(52):20024—20038. https://doi.org/10.1074/jbc.ra119.010740.

[10] Menzies, K.J., Zhang, H., Katsyuba, E., Auwerx, J., 2016. Protein acetylation in metabolism — metabolites and cofactors. Nature Reviews Endocrinology 12(1):43—60. https://doi.org/10.1038/nrendo.2015.181.

[11] Agathocleous, M., Meacham, C.E., Burgess, R.J., Piskounova, E., Zhao, Z., Crane, G.M., et al., 2017. Ascorbate regulates haematopoietic stem cell function and leukaemogenesis. Nature 549(7673):476—481. https://doi.org/10.1038/nature23876.

[12] Carey, B.W., Finley, L.W.S., Cross, J.R., Allis, C.D., Thompson, C.B., 2015. Intracellular α-ketoglutarate maintains the pluripotency of embryonic stem cells. Nature 518(7539):413—416. https://doi.org/10.1038/nature13981.

[13] Haensel, D., Jin, S., Sun, P., Cinco, R., Dragan, M., Nguyen, Q., et al., 2020. Defining epidermal basal cell states during skin homeostasis and wound healing using single-cell transcriptomics. Cell Reports 30(11):3932—3947.e6. https://doi.org/10.1016/j.celrep.2020.02.091.

[14] Hosseini, M., Dousset, L., Mahfouf, W., Serrano-Sanchez, M., Redonnet-Vernhet, I., Mesli, S., et al., 2018. Energy metabolism rewiring precedes UVB-induced primary skin tumor formation. Cell Reports 23(12):3621—3634. https://doi.org/10.1016/j.celrep.2018.05.060.

[15] Baksh, S.C., Todorova, P.K., Gur-Cohen, S., Hurwitz, B., Ge, Y., Novak, J.S.S., et al., 2020. Extracellular serine controls epidermal stem cell fate and tumour initiation. Nature Cell Biology 22(7):779—790. https://doi.org/10.1038/s41556-020-0525-9.

[16] Flores, A., Schell, J., Krall, A.S., Jelinek, D., Miranda, M., Grigorian, M., et al., 2017. Lactate dehydrogenase activity drives hair follicle stem cell activation. Nature Cell Biology 19(9):1017—1026. https://doi.org/10.1038/ncb3575.

[17] Villena, J.A., 2015. New insights into PGC-1 coactivators: redefining their role in the regulation of mitochondrial function and beyond. FEBS Journal 282(4):647—672. https://doi.org/10.1111/febs.13175.

[18] Zhang, Y., Shen, L., Zhu, H., Dreissigacker, K., Distler, D., Zhou, X., et al., 2020. PGC-1α regulates autophagy to promote fibroblast activation and tissue fibrosis. Annals of the Rheumatic Diseases 79(9):1227—1233. https://doi.org/10.1136/annrheumdis-2020-216963.

[19] Shoag, J., Haq, R., Zhang, M., Liu, L., Rowe, G.C., Jiang, A., et al., 2013. PGC-1 coactivators regulate MITF and the tanning response. Molecular Cell 49(1):145—157. https://doi.org/10.1016/j.molcel.2012.10.027.

[20] Crane, E.D., Wong, W., Zhang, H., O'Neil, G., Crane, J.D., 2021. AMPK inhibits mTOR-driven keratinocyte proliferation after skin damage and stress. Journal of Investigative Dermatology 141(9):2170—2177.e3. https://doi.org/10.1016/j.jid.2020.12.036.

[21] Crane, J.D., MacNeil, L.G., Lally, J.S., Ford, R.J., Bujak, A.L., Brar, I.K., et al., 2015. Exercise-stimulated interleukin-15 is controlled by AMPK and regulates

skin metabolism and aging. Aging Cell 14(4):625–634. https://doi.org/10.1111/acel.12341.

[22] Handschin, C., Choi, C.S., Chin, S., Kim, S., Kawamori, D., Kurpad, A.J., et al., 2007. Abnormal glucose homeostasis in skeletal muscle–specific PGC-1α knockout mice reveals skeletal muscle–pancreatic β cell crosstalk. Journal of Clinical Investigation 117(11):3463–3474. https://doi.org/10.1172/jci31785.

[23] Nakajima, K., Sano, S., 2018. Mouse models of psoriasis and their relevance. The Journal of Dermatology 45(3):252–263. https://doi.org/10.1111/1346-8138.14112.

[24] Schönwasser, D.C., Marais, R.M., Marshall, C.J., Parker, P.J., 1998. Activation of the mitogen-activated protein kinase/extracellular signal-regulated kinase pathway by conventional, novel, and atypical protein kinase C isotypes. Molecular and Cellular Biology 18(2):790–798. https://doi.org/10.1128/mcb.18.2.790.

[25] Mascré, G., Dekoninck, S., Drogat, B., Youssef, K.K., Brohée, S., Sotiropoulou, P.A., et al., 2012. Distinct contribution of stem and progenitor cells to epidermal maintenance. Nature 489(7415):257–262. https://doi.org/10.1038/nature11393.

[26] Cantó, C., Menzies, K.J., Auwerx, J., 2015. NAD+ metabolism and the control of energy homeostasis: a balancing act between mitochondria and the nucleus. Cell Metabolism 22(1):31–53. https://doi.org/10.1016/j.cmet.2015.05.023.

[27] Tan, C.L., Chin, T., Tan, C.Y.R., Rovito, H.A., Quek, L.S., Oblong, J.E., et al., 2019. Nicotinamide metabolism modulates the proliferation/differentiation balance and senescence of human primary keratinocytes. Journal of Investigative Dermatology 139(8):1638–1647.e3. https://doi.org/10.1016/j.jid.2019.02.005.

[28] Tran, M.T., Zsengeller, Z.K., Berg, A.H., Khankin, E.V., Bhasin, M.K., Kim, W., et al., 2016. PGC1α drives NAD biosynthesis linking oxidative metabolism to renal protection. Nature 531(7595):528–532. https://doi.org/10.1038/nature17184.

[29] Liu, L., Su, X., Quinn, W.J., Hui, S., Krukenberg, K., Frederick, D.W., et al., 2018. Quantitative analysis of NAD synthesis-breakdown fluxes. Cell Metabolism 27(5):1067–1080.e5. https://doi.org/10.1016/j.cmet.2018.03.018.

[30] Yoshino, J., Baur, J.A., Imai, S., 2017. NAD+ intermediates: the biology and therapeutic potential of NMN and NR. Cell Metabolism 27(3):513–528. https://doi.org/10.1016/j.cmet.2017.11.002.

[31] Chini, C.C.S., Zeidler, J.D., Kashyap, S., Warner, G., Chini, E.N., 2021. Evolving concepts in NAD+ metabolism. Cell Metabolism 33(6):1076–1087. https://doi.org/10.1016/j.cmet.2021.04.003.

[32] Wilk, A., Hayat, F., Cunningham, R., Li, J., Garavaglia, S., Zamani, L., et al., 2020. Extracellular NAD+ enhances PARP-dependent DNA repair capacity independently of CD73 activity. Scientific Reports 10(1):651. https://doi.org/10.1038/s41598-020-57506-9.

[33] Rouleau, M., Patel, A., Hendzel, M.J., Kaufmann, S.H., Poirier, G.G., 2010. PARP inhibition: PARP1 and beyond. Nature Reviews Cancer 10(4):293–301. https://doi.org/10.1038/nrc2812.

[34] Flores, I., Blasco, M.A., 2009. A p53-dependent response limits epidermal stem cell functionality and organismal size in mice with short telomeres. PLoS One 4(3):e4934. https://doi.org/10.1371/journal.pone.0004934.

[35] Missero, C., Cunto, F.D., Kiyokawa, H., Koff, A., Dotto, G.P., 1996. The absence of p21Cip1/WAF1 alters keratinocyte growth and differentiation and promotes ras-tumor progression. Genes & Development 10(23):3065–3075. https://doi.org/10.1101/gad.10.23.3065.

[36] Davalos, A.R., Kawahara, M., Malhotra, G.K., Schaum, N., Huang, J., Ved, U., et al., 2013. p53-dependent release of Alarmin HMGB1 is a central mediator of senescent phenotypesHMGB1 regulates the SASP. The Journal of Cell Biology 201(4):613–629. https://doi.org/10.1083/jcb.201206006.

[37] Nakajima, T., Nakashima, T., Okada, Y., Jo, M., Nishikawa, T., Mitsumoto, Y., et al., 2010. Nuclear size measurement is a simple method for the assessment of hepatocellular aging in non-alcoholic fatty liver disease: comparison with telomere-specific quantitative FISH and p21 immunohistochemistry. Pathology International 60(3):175–183. https://doi.org/10.1111/j.1440-1827.2009.02504.x.

[38] Langley, E., Pearson, M., Faretta, M., Bauer, U., Frye, R.A., Minucci, S., et al., 2002. Human SIR2 deacetylates p53 and antagonizes PML/p53-induced cellular senescence. The EMBO Journal 21(10):2383–2396. https://doi.org/10.1093/emboj/21.10.2383.

[39] Jiang, D., Vries, J.C., Muschhammer, J., Schatz, S., Ye, H., Hein, T., et al., 2020. Local and transient inhibition of p21 expression ameliorates age-related delayed wound healing. Wound Repair and Regeneration 28(1):49–60. https://doi.org/10.1111/wrr.12763.

[40] Albrecht, J.H., Meyer, A.H., Hu, M.Y., 1997. Regulation of cyclin-dependent kinase inhibitor p21(WAF1/Cip1/Sdi1) gene expression in hepatic regeneration. Hepatology (Baltimore, Md.) 25(3):557–563.

[41] Surjana, D., Halliday, G.M., Damian, D.L., 2013. Nicotinamide enhances repair of ultraviolet radiation-induced DNA damage in human keratinocytes and ex vivo skin. Carcinogenesis 34(5):1144–1149. https://doi.org/10.1093/carcin/bgt017.

[42] Katayoshi, T., Nakajo, T., Tsuji-Naito, K., 2021. Restoring NAD+ by NAMPT is essential for the SIRT1/p53-mediated survival of UVA- and UVB-irradiated epidermal keratinocytes. Journal of Photochemistry and Photobiology B: Biology 221:112238. https://doi.org/10.1016/j.jphotobiol.2021.112238.

[43] Chen, A.C., Martin, A.J., Choy, B., Fernández-Peñas, P., Dalziell, R.A., McKenzie, C.A., et al., 2015. A phase 3 randomized trial of nicotinamide for skin-cancer chemoprevention. New England Journal of Medicine 373(17):1618–1626. https://doi.org/10.1056/nejmoa1506197.

[44] Malesu, R., Martin, A.J., Lyons, J.G., Scolyer, R.A., Chen, A.C., McKenzie, C.A., et al., 2020. Nicotinamide for skin cancer chemoprevention: effects of nicotinamide on melanoma in vitro and in vivo. Photochemical and Photobiological Sciences 19(2):171–179. https://doi.org/10.1039/c9pp00388f.

[45] Sahin, E., Colla, S., Liesa, M., Moslehi, J., Müller, F.L., Guo, M., et al., 2011. Telomere dysfunction induces metabolic and mitochondrial compromise. Nature 470(7334):359–365. https://doi.org/10.1038/nature09787.

[46] Xiong, S., Patrushev, N., Forouzandeh, F., Hilenski, L., Alexander, R.W., 2015. PGC-1α modulates telomere function and DNA damage in protecting against aging-related chronic diseases. Cell Reports 12(9):1391–1399. https://doi.org/10.1016/j.celrep.2015.07.047.

[47] Caporarello, N., Meridew, J.A., Jones, D.L., Tan, Q., Haak, A.J., Choi, K.M., et al., 2019. PGC1α repression in IPF fibroblasts drives a pathologic metabolic, secretory and fibrogenic state. Thorax 74(8):749–760. https://doi.org/10.1136/thoraxjnl-2019-213064.

[48] Velarde, M.C., Demaria, M., Melov, S., Campisi, J., 2015. Pleiotropic age-dependent effects of mitochondrial dysfunction on epidermal stem cells. Proceedings of the National Academy of Sciences 112(33):10407–10412. https://doi.org/10.1073/pnas.1505675112.

[49] Park, J., Halliday, G.M., Surjana, D., Damian, D.L., 2010. Nicotinamide prevents ultraviolet radiation-induced cellular energy loss. Photochemistry and Photobiology 86(4):942–948. https://doi.org/10.1111/j.1751-1097.2010.00746.x.

[50] Kiss, B., Szántó, M., Hegedűs, C., Antal, D., Szödényi, A., Márton, J., et al., 2020. Poly(ADP-ribose) polymerase-1 depletion enhances the severity of inflammation in an imiquimod-induced model of psoriasis. Experimental Dermatology 29(1):79–85. https://doi.org/10.1111/exd.14061.

[51] El-Hamoly, T., Hegedűs, C., Lakatos, P., Kovács, K., Bai, P., El-Ghazaly, M.A., et al., 2014. Activation of poly(ADP-ribose) polymerase-1 delays wound

healing by regulating keratinocyte migration and production of inflammatory mediators. Molecular Medicine 20(1):363—371. https://doi.org/10.2119/molmed.2014.00130.

[52] Wiley, C.D., Velarde, M.C., Lecot, P., Liu, S., Sarnoski, E.A., Freund, A., et al., 2015. Mitochondrial dysfunction induces senescence with a distinct secretory phenotype. Cell Metabolism 23(2):303—314. https://doi.org/10.1016/j.cmet.2015.11.011.

[53] Covarrubias, A.J., Kale, A., Perrone, R., Lopez-Dominguez, J.A., Pisco, A.O., Kasler, H.G., et al., 2020. Senescent cells promote tissue NAD+ decline during ageing via the activation of CD38+ macrophages. Nature Metabolism 2(11):1265—1283. https://doi.org/10.1038/s42255-020-00305-3.

[54] Chini, C.C.S., Peclat, T.R., Warner, G.M., Kashyap, S., Espindola-Netto, J.M., de Oliveira, G.C., et al., 2020. CD38 ecto-enzyme in immune cells is induced during aging and regulates NAD+ and NMN levels. Nature Metabolism 2(11):1284—1304. https://doi.org/10.1038/s42255-020-00298-z.

[55] Shats, I., Williams, J.G., Liu, J., Makarov, M.V., Wu, X., Lih, F.B., et al., 2020. Bacteria boost mammalian host NAD metabolism by engaging the deamidated biosynthesis pathway. Cell Metabolism 31(3):564—579.e7. https://doi.org/10.1016/j.cmet.2020.02.001.

[56] Alston, T.A., Abeles, R.H., 1988. Substrate specificity of nicotinamide methyltransferase isolated from porcine liver. Archives of Biochemistry and Biophysics 260(2):601—608. https://doi.org/10.1016/0003-9861(88)90487-0.

[57] Demaria, M., Ohtani, N., Youssef, S.A., Rodier, F., Toussaint, W., Mitchell, J.R., et al., 2014. An essential role for senescent cells in optimal wound healing through secretion of PDGF-AA. Developmental Cell 31(6):722—733. https://doi.org/10.1016/j.devcel.2014.11.012.

[58] Liu, N., Matsumura, H., Kato, T., Ichinose, S., Takada, A., Namiki, T., et al., 2019. Stem cell competition orchestrates skin homeostasis and ageing. Nature 568(7752):344—350. https://doi.org/10.1038/s41586-019-1085-7.

[59] Azazmeh, N., Assouline, B., Winter, E., Ruppo, S., Nevo, Y., Maly, A., et al., 2020. Chronic expression of p16INK4a in the epidermis induces Wnt-mediated hyperplasia and promotes tumor initiation. Nature Communications 11(1):2711. https://doi.org/10.1038/s41467-020-16475-3.

[60] Donati, G., Watt, F.M., 2015. Stem cell heterogeneity and plasticity in epithelia. Cell Stem Cell 16(5):465—476. https://doi.org/10.1016/j.stem.2015.04.014.

